Applied Clay Science 238 (2023) 106923

Contents lists available at ScienceDirect

Applied Clay Science

journal homepage: www.elsevier.com/locate/clay

Research Paper

Alteration of trioctahedral micas in the presence of inorganic and organic acids

Chiara Cappelli [a,1], Alexander E.S. Van Driessche [a], Jordi Cama [b], F. Javier Huertas [a,*]

[a] Instituto Andaluz de Ciencias de la Tierra – IACT (CSIC-University of Granada), 18100 Armilla, Granada, Spain
[b] Institute of Environmental Assessment and Water Research (IDAEA), CSIC, 08034 Barcelona, Catalonia, Spain

ARTICLE INFO

Keywords:
Laser confocal microscopy
Interferometry
AFM
Dissolution
Organic acid
Mica
Biotite
Phlogopite

ABSTRACT

The alteration of two trioctahedral micas, biotite and phlogopite, was investigated at the meso, micro, and nanoscale using three complementary microscopy techniques to better understand mica surface reactivity. In situ and ex situ experiments were performed to monitor the mineral interface during dissolution in acidic solutions (nitric and oxalic acid, pH ~ 1–2), over a temperature range of 25–100°C. The inorganic acid was used as a benchmark condition to elucidate the effect of the organic acid on the dissolution behavior. The observed topographical changes that arose during mineral alteration revealed the simultaneous occurrence of different processes that heterogeneously shaped the mica surface: 1) the retreat of pre-existing and newly formed steps (edge surface reactivity). In the case of biotite, layer curling and peeling-off occurred in the presence of nitric acid whereas dendritic-shaped step edges resulted from the effect of oxalic acid; 2) the nucleation of etch pits and the formation of dissolution channels on the (001) surface. Oxalic acid promoted the growth of the pits to such an extent that they were discernible at each scale and resolution investigated; and 3) precipitation of secondary phases. Overall, a multi-scale approach offers new insights into the dissolution behavior of biotite versus phlogopite and provides and enhances understanding of the effect that oxalic acid has on the surface reactivity of mica.

1. Introduction

Micas are ubiquitous phyllosilicate minerals in the Earth's crust, present in metamorphic, sedimentary, and igneous rocks (Ottolini et al., 2010). Their low-temperature surface alteration through dissolution and/or vermiculization has important implications for a variety of fields, from soil and agro-environmental sciences (Aoudjit et al., 1996; McMaster et al., 2008; Bonneville et al., 2011; Arocena et al., 2012; Voinot et al., 2013; Li et al., 2015; Pinzari et al., 2016; Said et al., 2018) to geological CO_2 sequestration and the carbon cycle (Hu et al., 2011; Shao et al., 2011a, 2011b; Garcia et al., 2012; Zhang et al., 2017; Min et al., 2018; Balland-Bolou-Bi et al., 2019), treatment of mine tailings and remediation of nuclear-fuel contaminated soil and groundwater (Wu et al., 2018; Niu et al., 2020). The dependence of trioctahedral mica surface reactivity as a function of environmental variables (pH, temperature, solution composition) has been extensively studied. It has been shown that dissolution of (hk0) mineral edge surfaces dominates over less reactive (001) basal surfaces, for micas altered with inorganic acids and over a wide range of pH and temperature (pH ~ 1–9.5, T ~ 11–105°C; Acker and Bricker, 1992; Kaviratna and Pinnavaia, 1994; Turpault and Trotignon, 1994; Rufe and Hochella, 1999; Hodson, 2006; Cappelli et al., 2013; Cappelli et al., 2015). Other studies, however, reported a significant contribution of the (001) surface to the overall mineral dissolution, especially in the presence of oxalic acid and/or under critical conditions (e.g., pH = 1.3–3.2, T ~ 10–200°C and supercritical CO_2; Aldushin et al., 2006; Haward et al., 2011; Garcia et al., 2012; Pachana et al., 2012; Lamarca-Irisarri et al., 2019; Cappelli et al., 2020). The reason for this apparent difference between laboratory observations remains elusive, and as such a consensus about the reactivity of micas has not been reached, although it has been claimed that etch pits generated from screw dislocations play a dominant role in phyllosilicate dissolution (Kurganskaya and Luttge, 2013).

In this study, the reactivity of biotite and phlogopite (trioctahedral micas) was investigated at pH ~1–2 in the presence of inorganic (HNO_3)

* Corresponding author.
E-mail address: javier.huertas@csic.es (F.J. Huertas).
[1] Present address: MAiMA group, Department of Mineralogy, Petrology and Applied Geology, University of Barcelona (UB), Martí Franquès s/n, 08028 Barcelona, Spain.

https://doi.org/10.1016/j.clay.2023.106923
Received 2 December 2022; Received in revised form 15 March 2023; Accepted 20 March 2023
Available online 28 March 2023

and organic ($H_2C_2O_4$) acids over a temperature range between 25 and 100°C. Under these conditions, laser confocal differential interference microscopy (LCM-DIM), vertical scanning and phase shifting interferometry (VSI-PSI), and atomic force microscopy (AFM) were used to monitor the evolution of the mica surface morphology and topography. This combination of meso- to nanoscale observations of the reacting water-mineral interface allows us to achieve a global vision of the variability of the weathering processes for the same mineral, between different mica members, and most importantly between two different acids. The inorganic acid was used here as a benchmark system to elucidate the effects and variations due to the presence of an organic acid on mica dissolution. This is important because organic acids, such as small carboxylic acids, are ubiquitous in soils and sediments. Particularly, oxalic acid that predominantly originates from root exudation, plant decomposition, and fungi or bacteria activity, plays an important catalyzing role in mineral weathering (Studenroth et al., 2013).

Therefore, to more comprehensively assess the role that micas play in (bio)geochemical processes, it is essential to improve our understanding of the reactions that take place at the mineral interface. In addition, the investigation of the reactivity of micas, whose flake size allows the accurate examination of the surface-solution interface, provides information on the dissolution mechanisms of other nano and microscopic phyllosilicates belonging to clays and clay minerals. Recent studies aimed to elucidate the reactions driving the dissolution of clay minerals at a molecular and atomic level (Schabernack et al., 2021; Schliemann and Churakov, 2021). Notably, the predicted heterogeneity of a mineral's reactivity through space and time has been successfully compared with nano-topographical observations of the interface of mica minerals obtained by high-resolution microscopy techniques (Luttge et al., 2019; Kurganskaya and Luttge, 2021). In this study, the reactivity of biotite and phlogopite was compared using a multi-scale observational approach. The influence of oxalic acid on the dissolution of both (hk0) and (001) mica faces was investigated, and an attempt to describe the complexity of the processes involved in mica alteration is provided. This knowledge is critical to appropriately interpreting the phyllosilicate reactivity under different environmental conditions and provides critical data for the future implementation of predictive numerical modelling.

2. Materials and methods

2.1. Sample characterization

Samples of phlogopite from Templeton (Ontario, Canada) and biotite from Bancroft (Ontario, Canada) were obtained through Ward's Natural Science Establishment. A detailed chemical and mineralogical characterization (Fig. SI1) of both samples was included as Supplementary Information. Samples consist of pure mica with trace inclusions of accompanying mineral phases (e.g., rutile, zircon, Figs. SI2-SI3), that should not affect the mica surface during alteration experiments (note that their presence was not detected by XRD). The chemical composition of mica crystals free of inclusions of accessory minerals was determined by transmission and analytical electron microscopy (TEM-AEM) (see Supplementary Information). Considering that all iron was in the form of Fe^{II}, the structural formula can be calculated as follows:

$$\text{Phlogopite}: K_{0.93}(Mg_{2.63}Fe_{0.15}Al_{0.16})(Al_{1.03}Si_{2.97})O_{10}(OH)_2$$

$$\text{Biotite}: K_{0.97}(Mg_{1.40}Fe_{1.29}Al_{0.04}Ti_{0.09}Mn_{0.09})(Al_{0.97}Si_{3.03})O_{10}(OH)_2$$

Flakes of biotite and phlogopite with a cleaved (001) surface of approximately 100 mm^2 and 0.08–0.15 mm thick were placed in batch reactors and retrieved at different reaction times for ex situ VSI/PSI measurements.

Biotite flakes with (001) cleavage surfaces of approximately 16 mm^2 and 0.08–0.15 mm thick were used in flow-through experiments for in situ LCM-DIM monitoring. In addition, ex situ AFM observations (Bruker Nanoscope III) were performed on freshly cleaved and reacted biotite and phlogopite flakes of 0.25 mm^2 and 0.08–0.15 mm thick. Measurements were performed at room temperature (23 ± 1°C), in contact mode using nonconductive silicon nitride uncoated tips (Bruker).

2.2. Experimental setup

2.2.1. Ex situ observations

Batch experiments were performed to study phlogopite and biotite dissolution in the presence of inorganic (HNO_3) and organic (oxalic acid; $H_2C_2O_4$) acids over a temperature range of 25–100°C (Table 1). Higher temperatures were used for the phlogopite (Px experiment series) to obtain faster phlogopite dissolution rates ensuring surface topographical changes comparable with those on biotite (Bx series). Similarly, some experiments at lower temperatures for both the Px and Bx, were allowed to react longer in order to attain observable surface changes. All solutions were prepared from ultrapure-grade chemicals and Milli-Q water. A 0.01 mol L^{-1} $NaNO_3$ solution was used as the background electrolyte. Sample flakes were placed in polyethylene bottles filled with 250 mL of solution. A freshly cleaved flake was used for each experiment. The temperature was held constant by means of a thermostatic bath or oven with high accuracy control (± 1°C). At the end of each experiment, the samples were retrieved, washed with Milli-Q water, and dried at room temperature. Ex situ observations of morphological and topographical changes in phlogopite and biotite [001]-oriented flakes were performed using interferometric techniques (vertical scanning (VSI) and phase shifting (PSI) interferometry) and AFM (Table 1).

2.2.2. In situ observations

Biotite flakes were placed in a custom-built flow-through cell attached to the LCM-DIM system so that the surface reactivity of the (001) surface could be effectively monitored in situ (see Cappelli et al., 2013 and Van Driessche and Sleutel, 2013 for specifics about the technique and the experimental set-up) during dissolution with 0.1 mol L^{-1}

Table 1
Conditions of ex situ (VSI/PSI, AFM) and in situ (LCM-DIM) dissolution experiments for phlogopite (P) and biotite (B); ox = oxalic acid.

pH	experiment	Temperature (°C)	duration (h)	HNO_3 (mol L^{-1})	$H_2C_2O_4$ (mol L^{-1})
VSI/PSI					
1.0	P1	40	1056	0.1	
	P2	70	168	0.1	
	P3	100	48	0.1	
	P4	100	96	0.1	
	B1	70	248	0.1	
2.0	P5	70	144	0.01	
	P6	100	24	0.01	
	P6	100	48	0.01	
1.3	P1ox	70	168		0.1
	P2ox	80	48		0.1
	B1ox	25	1656		0.1
	B2ox	40	72		0.1
	B3ox	40	120		0.1
	B4ox	50	72		0.1
2.1	P3ox	70	168		0.01
	P4ox	80	48		0.01
	B5ox	25	816		0.01
	B6ox	40	72		0.01
	B7ox	40	192		0.01
	B8ox	50	192		0.01
	B9ox	70	72		0.01
AFM					
1.0	B1afm	70	72	0.1	
1.3	P1afm-ox	40	72		0.1
	B1afm-ox	40	72		0.1
	B2afm-ox	70	24		0.1
LCM-DIM					
1.3	B1LD	25	93		0.1
	B2LD	50	18		0.1

oxalic acid (pH 1.3) solution and 0.01 mol L^{-1} $NaNO_3$ as background electrolyte. All solutions were prepared from ultrapure-grade chemicals and Milli-Q water. Two experiments were performed at 25°C and 50°C, over a total time of 93 and 18 h, respectively (Table 1). Images of the (001) cleavage surface were taken every 20 s with a capture time of 9.6 s.

3. Results

3.1. Phlogopite dissolution in the presence of nitric acid

The freshly cleaved surface of the phlogopite sample appeared heterogeneous, with several bulges and cracks covering part of the surface

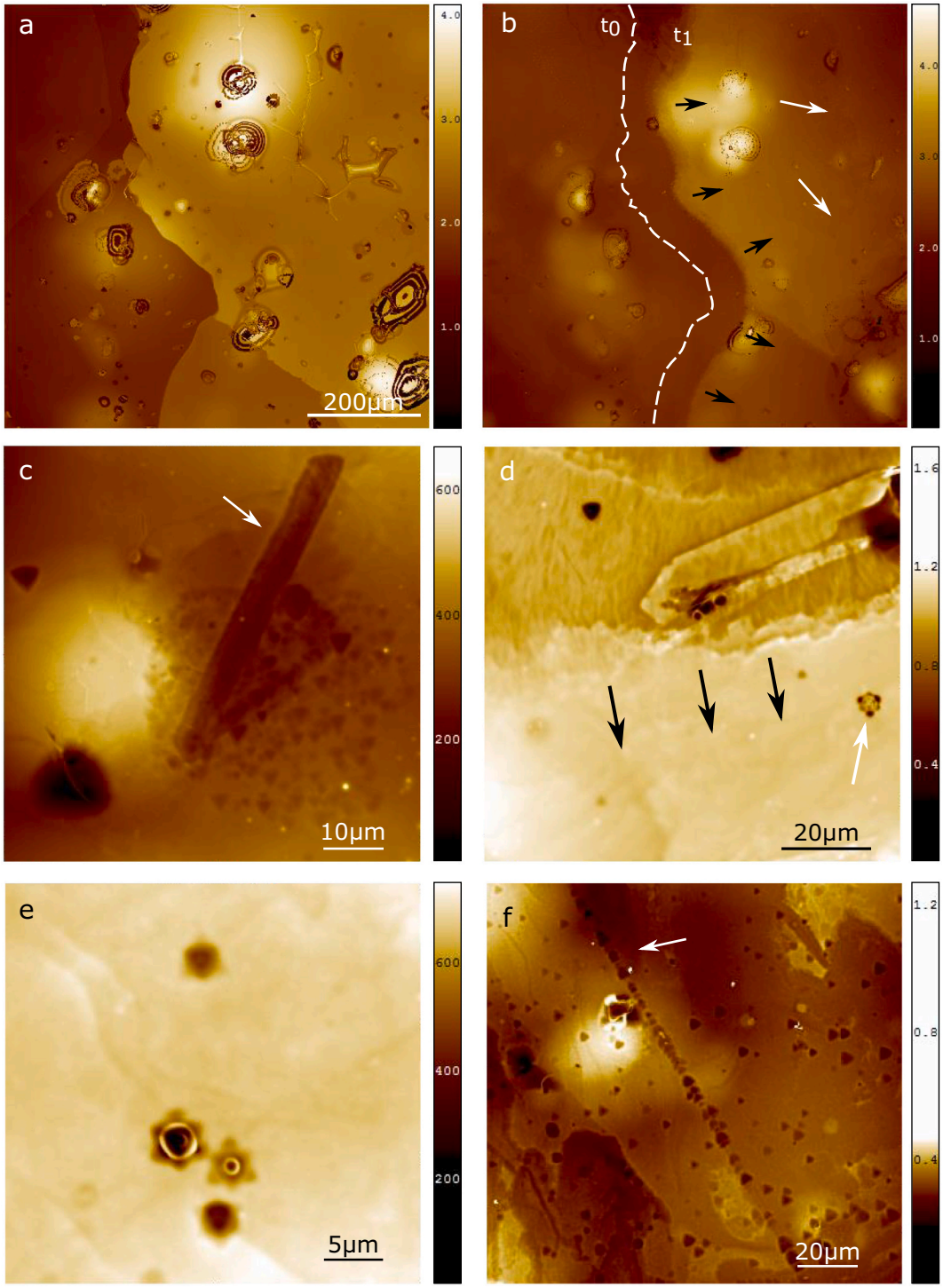

Fig. 1. VSI images of phlogopite (001): (a) unreacted surface and (b-f) surfaces reacted with 0.1 mol L^{-1} HNO_3 (pH 1). In (a), terraces (the brighter the color the higher the terrace) with bulges and cracks were observed. After reaction at 100°C for 96 h (b), the main edge (dotted line) retreated from t_0 to t_1 moving right (black arrows); additional reaction fronts formed on the main terrace (white arrows). At 70°C for 168 h (c-e) etch pits developed either dispersed on the surface, or intensely etching specific areas or aligned forming trenches (white arrow in (c)). Retreat of reaction fronts (step edges) always occurred (black arrows in (d)). The coalescence of small etch pits leads to hexagonal shaped structures (white arrow in (d)) or formed six-tip stars (e). At 100°C for 48 h (f) the dissolution is intense (larger etch pit size and higher density). Long trenches of aligned and coalesced etch pits formed (white arrow). Same x-y scale in (a) and (b). z scale in µm (a,b,d,f) and nm (c,e).

(VSI image, Fig. 1a). During the dissolution experiments within the HNO_3 solution, these structures enhanced the reactivity of the basal surface, leading to a surface roughening and generation of new reaction fronts (Fig. 1b). On the other hand, the mineral inclusions identified by scanning electron microscopy and optical microscopy (Supplementary Information) did not observably contribute to the phlogopite dissolution processes.

Step retreat (Fig. 1a,b and Fig. SI4) and triangular etch pits (Fig. 1c-f) were identified as the main dissolution features of phlogopite alteration. The etch pits were heterogeneously distributed over the phlogopite (001) surface (c.f., Fig. 1c) showing variable size and density and the same orientation. In some areas, they were highly dispersed (i.e., low pit density), while in other areas etch pit coalescence was observed (side from 0.7 to 6 μm, after reaction with 0.1 mol L^{-1} HNO_3 at 70°C for 168 h; Fig. 1c) yielding intensively etched areas. Moreover, etch pits of similar size and alignment tend to coalesce forming relatively long trenches (56 to 80 μm long) (Fig. 1c,f). In some instances, the coalescence of these etch pits resulted in hexagonal-shaped structures (white arrow in Fig. 1d). Similarly, the apparent overlapping of triangular etch pits with opposite orientations (Fig. 1e) likely formed as the result of the coalescence of smaller etch pits. Etch pit nucleation and growth increased with temperature, resulting in a higher pit density (Fig. 1f) and larger etch pits (average size of up to ~4.5 μm). New generations of etch pits formed continuously as preexisting ones grew during the experimental time-lapse.

In the P4 experiment (HNO_3 solution at pH 1 and 100°C; Table 1), a step-retreat rate (dissolution of (hk0) surfaces; R_{step} in μm s^{-1}) was obtained by comparing VSI images of unreacted and reacted surfaces (Fig. 1a,b) and a horizontal step retreat at a given location of the surface was calculated as:

$$R_{step} = \frac{\Delta L}{(t_2 - t_1)} \quad (2)$$

where ΔL is the change in the surface horizontal length between t_0 and t_1 at a given location. A calculated average R_{step} value of 2.35×10^{-4} μm s^{-1} was 3 orders of magnitude slower than the estimated value of 5×10^{-1} μm s^{-1} for the biotite dissolution rate at pH 1 and 100°C, derived by applying the Arrhenius law using the LCM-DIM retreat rate measured at 25°C and the apparent energy value ($E_a = 62$ kJ mol^{-1}) as reported by Cappelli et al. (2013, 2020)

At pH 2 and 100°C, small rectangular (< 5 μm) and big rounded (< 30 μm)) precipitates formed on the phlogopite surface (Fig. SI5). The composition of these secondary phases is unknown.

3.2. Phlogopite dissolution in the presence of oxalic acid

In the presence of oxalic acid and similarly to the alteration observed

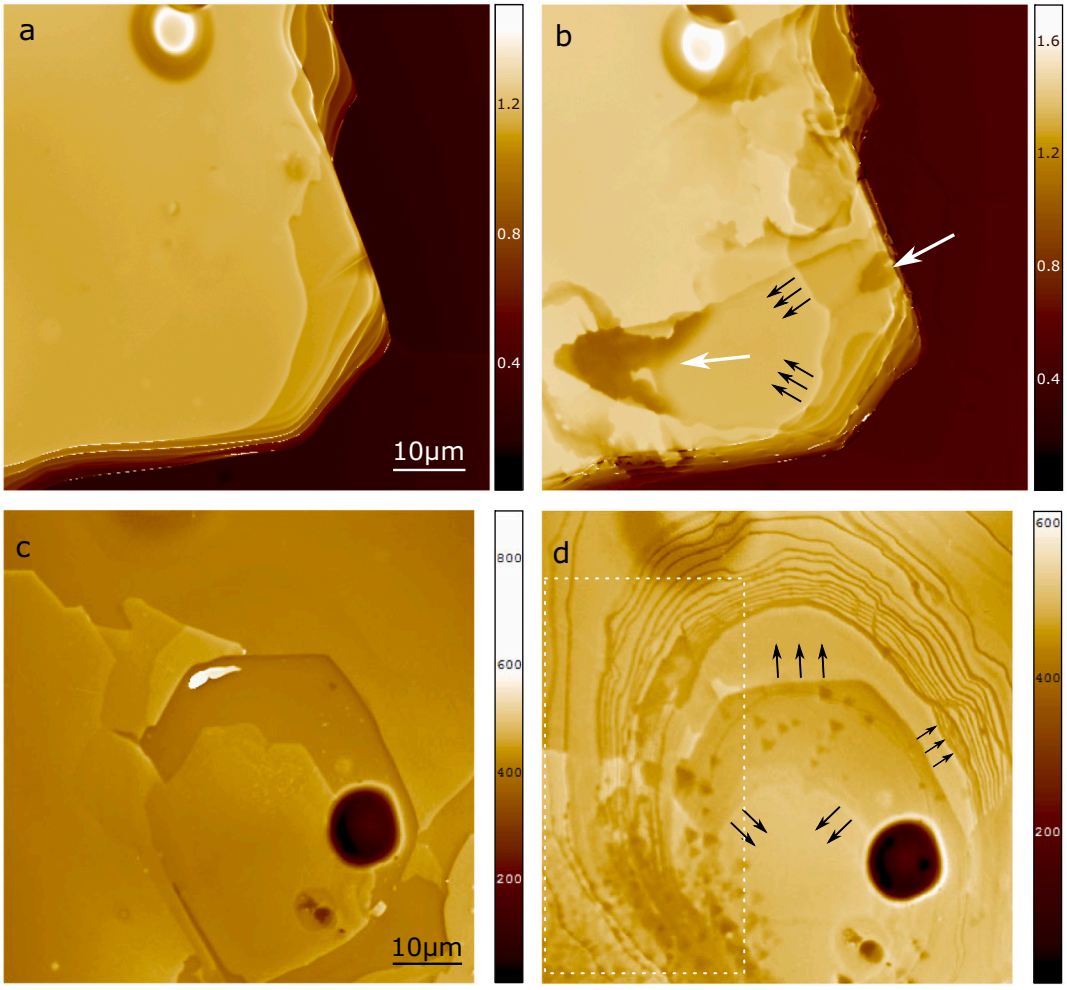

Fig. 2. VSI images of phlogopite (001): (a,c) unreacted surface and (b,d) after reaction with 0.01 mol L^{-1} oxalic acid at 70°C for 168 h. Several reaction fronts moved inwards (black arrows in (b) and (d)) mostly perpendicularly to the step edge although irregular dissolution fronts moved underneath the uppermost layers (white arrows in (b)) in some areas. Intense dissolution of the uppermost terraces led to their almost disappearance from the field of view (white dotted box in (d)). Dissolution channels formed almost parallel to the step direction of the main (central) terrace and etch pits nucleated heterogeneously (d). x-y scale in (b) and (d) same as (a) and (c), respectively. z scale in μm (a,b) and nm (c,d).

in nitric acid solution, the phlogopite edge surface retreat and basal surface etching were the main processes detected during dissolution (Figs. 2 and 3). Moreover, several dissolution channels were formed in the alteration process (Fig. 2d). It should also be noted that in several instances etch pits formed within the channels, where reactivity is likely higher (Fig. SI6).

As in nitric acid, the basal surface etching was heterogeneous, yielding areas with intense etch pit nucleation (etch pit sides from ~1 to 6 μm; Fig. 3). An increase in the concentration of oxalic acid from 0.01 to 0.1 mol L^{-1} enhanced the etch pit nucleation and growth (Fig. 3c,d).

AFM imaging showed an incipient formation of the triangular etch pits (size from 20 to 100 nm) that formed in the presence of 0.1 mol L^{-1} oxalic acid at 40°C after 72 h (Fig. SI7).

3.3. Biotite dissolution in the presence of nitric acid

Ex situ VSI observations of reacted biotite (001) surface in the presence of 0.1 mol L^{-1} of nitric acid (pH ~ 1) at 70°C showed that swelling and peeling of the edges of high steps and retreat of the edge surface were the main processes driving biotite dissolution (Fig. SI8; see also Cappelli et al., 2013, 2020). Likewise, several dissolution channels formed in some areas resulting in a cracked basal surface (Fig. SI8b-c). Despite a severe degradation of the biotite (001) surface, etch pits were not identified.

AFM images of the basal surface reacted in 0.1 mol L^{-1} HNO_3 solution and 70°C showed the formation of small etch pits (20–100 nm wide and ~ 3 nm deep) (Fig. 4). This finding complements the VSI data of this study and previous studies by Cappelli et al. (2013, 2020), who did not observe etching of biotite basal surface monitored by interferometry and LCM-DIM during dissolution at pH 1–3 (HNO_3) and 11–80°C.

3.4. Biotite dissolution in the presence of oxalic acid

In situ experiments performed in the presence of 0.1 mol L^{-1} oxalic acid (pH ~ 1.3) at 25 and 50°C showed the formation of irregular dendritic dissolution structures that spread from the step edges, and the development of large hexagonal structures (e.g., side of ~35 and 62 μm after reaction in 0.1 mol L^{-1} oxalic acid solution at 25°C (93 h) and 50°C (18 h) respectively) (Figs. 5, 6a,b and Fig. SI9). Some areas of the biotite surface exhibited evidence of dissolution at 50°C whereby dendritic structures started to grow rapidly from the edge surface and eventually developed a hexagonal shaped structure (Fig. 5). At this point, dissolution from the hexagonal etch pits edges nearly stopped, while it continued from preexisting step edges (see Supplementary material LCM-DIM-Movie1 and LCM-DIM-Movie2).

A few small rounded etch pits were observed by LCM-DIM. However, PSI ex situ observations of the sample after the flow-through experiment showed the presence of etch pits over the entire surface (Fig. 6a,b).

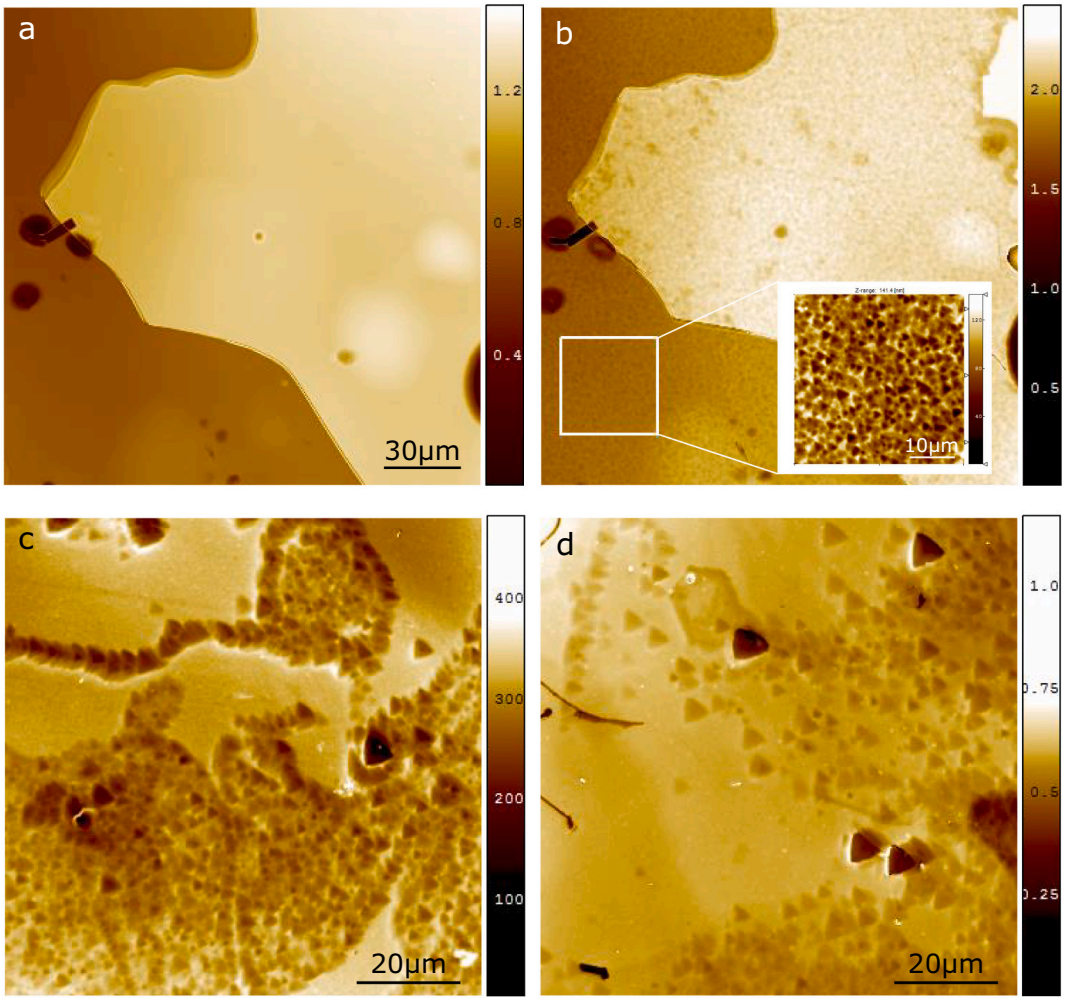

Fig. 3. VSI images of phlogopite (001): (a) unreacted surface and surface after reaction with (b) 0.01 mol L^{-1} and (c,d) 0.1 mol L^{-1} oxalic acid at 70°C for 168 h. Intense etching altered extensive areas of the surface (b). The size range of the etch pits increased with increasing oxalic acid concentration (from ~1–3 μm at 0.01 mol L^{-1} to ~1–6 μm at 0.1 mol L^{-1} oxalic acid). Etch pits often aligned and coalesced forming trenches (c,d). Same x-y scale in (a) and (b). z scale in nm (c) and μm (a,b,d).

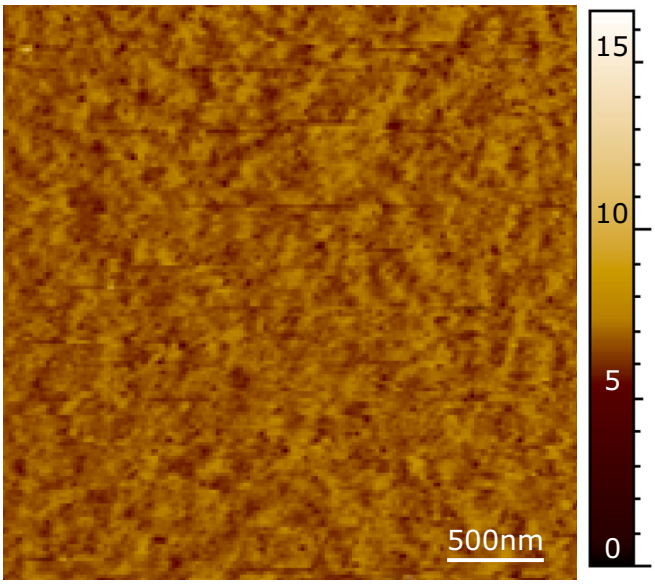

Fig. 4. AFM image of the biotite (001) surface reacted at pH 1 (HNO_3) and 70 °C for 72 h. Etch pits (dark spots ~20–100 nm wide and ~ 3 nm deep) formed uniformly over the surface. z scale in nm.

Similarly, ex situ VSI observations of the biotite (001) surface (Fig. 6c-f and Figs. 7 and SI10) reacted with oxalic acid (0.01–0.1 mol L^{-1}) at 25–70°C revealed dendritic dissolution patterns at the step edges and formation of a heterogeneous population of etch pits. Small, rounded pits (diameter < 2 μm) formed over the entire basal surface while large etch pits (22–135 μm; Fig. 7) only originated in some areas. These large etch pits exhibited circular or pseudo-hexagonal shaped structures for biotite reacted with 0.01 mol L^{-1} oxalic acid at different temperatures (Figs. 6e and 7a-d), whereas an increase in oxalic acid concentration to 0.1 mol L^{-1} led to the formation of well-defined hexagonal etch pits (Figs. 7f and SI10; see also Fig. 6a,b). It should also be noted that the dendritic features became more evident as the temperature and the oxalic acid concentration decreased (Fig. 6c-f), displaying an apparent preferred propagation orientation in some cases (Fig. 6e).

Regardless of the shape and step edge morphology of large etch pits (Fig. 7b-f), in some cases steps propagate from the pit walls as proposed in the stepwave model where trains of steps periodically generate from an etch pit originated by a screw dislocation (Lasaga and Luttge, 2001).

In agreement with the VSI and LCM-DIM observations, AFM images of biotite reacting with 0.1 mol L^{-1} oxalic acid (Fig. 8) showed dendritic step edge dissolution, small ~rounded etch pits (~ 5–15 nm) and pseudo hexagonal etch pits with stepwave patterns. Moreover, precipitates coated some areas of the surface after 24 h of reaction at 70°C (Fig. 8c).

4. Discussion

4.1. Phlogopite vs biotite dissolution

Although similar processes drive the dissolution of biotite and phlogopite in acidic conditions, i.e., step retreat (lateral (hk0) dissolution) and etch pit formation on the basal (001) surface, important differences were observed between the topographical changes of the two micas. The first noticeable difference is related to the phenomena associated with the step edge retreat. Swelling and peeling of the uppermost mineral layers described for biotite (Fig. SI8 and Fig. 1 in Cappelli et al., 2020), was never observed during phlogopite dissolution under the experimental conditions of the present study. Secondly, the basal plane reactivity of phlogopite was similar under all the studied alteration conditions (i.e., triangular etch pits formed and developed

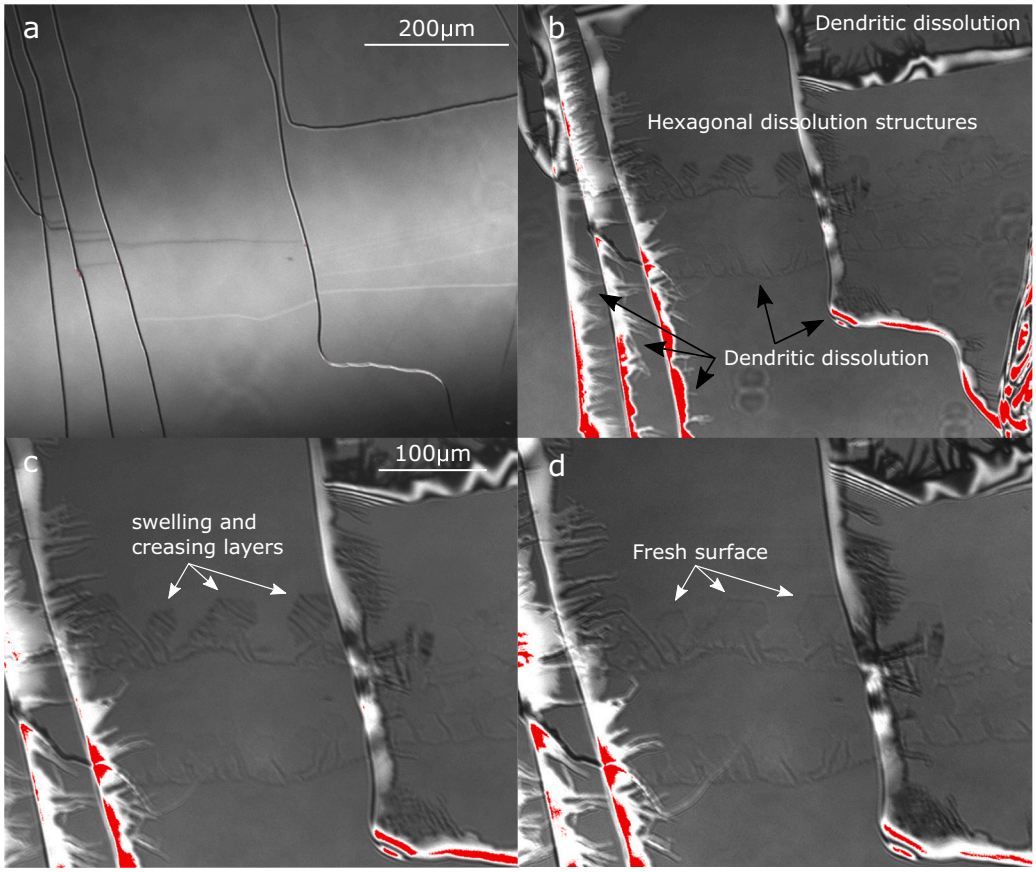

Fig. 5. LCM-DIM images of biotite (001) (a) unreacted surface and same surface after reaction in 0.1 mol L^{-1} oxalic acid solution (pH 1.3) at 25°C for (b) ~ 68 h; (c) ~ 72 h and (d) ~ 93 h. Terraces are delimited by steps (observed as lines); the higher the contrast the higher the steps between terraces. Dissolution started along the step edges (black arrows in (b)) resulting in dendritic features. Hexagonal shaped structures formed at the apex of those structures after specific reaction times (b-d). Scale in (b) and (d) same as (a) and (c), respectively.

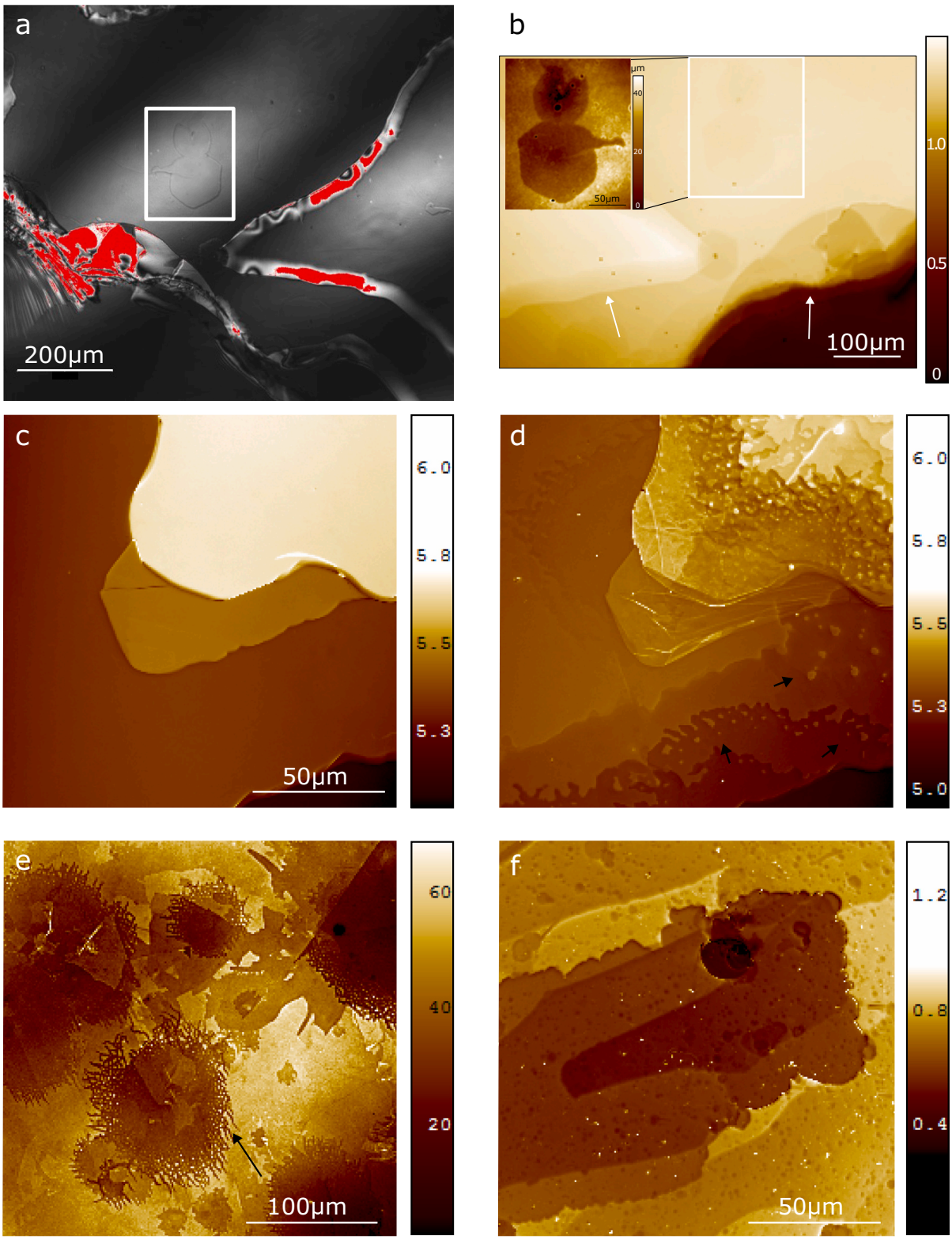

Fig. 6. Images of biotite (001) surface reacted with oxalic acid at different temperatures. (a) LCM-DIM image after reaction with 0.1 mol L^{-1} oxalic acid at 50°C for 18 h and (b) same surface displayed by PSI after sample retrieving. Large hexagonal (~40–50 µm) and smaller rounded (~6 µm) etch pits formed. Step retreat (white arrows in (b)) took place after edge roughening (high contrast areas in (a)). White boxes in (a) and (b) delimit the area depicted in the inset in (b). (c) VSI image of an unreacted surface and (d) same surface after reaction with 0.01 mol L^{-1} oxalic acid at 40 °C for 72 h. Small islands of material formed after dendritic dissolution (black arrows in (d)). (e) VSI image after reaction with 0.01 mol L^{-1} oxalic acid at 25°C for 816 h. Black arrow indicates possible crystallographic orientation of the branches. (f) VSI image after reaction with 0.1 mol L^{-1} oxalic at 25°C for 1656 h. Jugged shaped dissolution edges formed as the oxalic acid concentration increased (pH decrease). x-y scale in (d) same as (c). z scale in nm (e) and µm in the rest of the images.

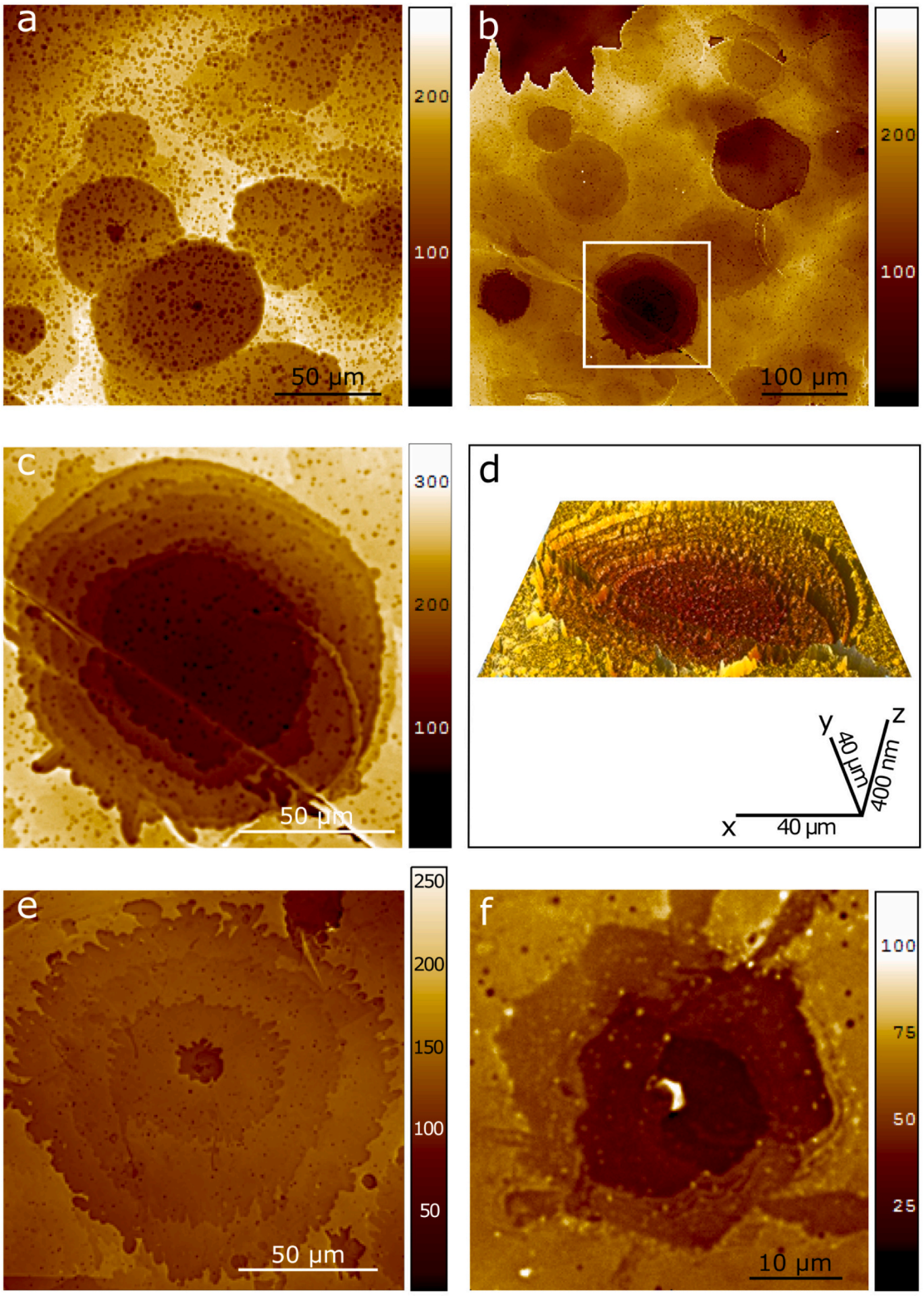

Fig. 7. VSI images of biotite (001) surface reacted with (a-e) 0.01 and (f) 0.1 mol L^{-1} oxalic acid at different temperatures. (a) Intense etching after 72 h at 70°C. Large rounded (~ 22–65 µm) and smaller (from hundreds of nm to ~3 µm) etch pits formed. At 50 °C during 192 h (b-d) the large etch pits (~50–115 µm) display a pseudo-hexagonal shaped structure, small etch pits of diameter < 3 µm covered the surface and dendritic dissolution patterns are visible. The white box in (b) delimits the etch pit depicted in (c) and (d) (3D view), where the stepwave process is evident (see text for details). At lower temperature ((e), 40 °C for 192 h), larger etch pits formed (~ 135 µm) followed by stepwaves, the small etch pits had a diameter < 2 µm and dendritic dissolution from the step edges created deeper branches. An increase of the oxalic acid concentration (f) led to the formation of hexagonal etch pits after reaction at 40°C for 72 h. Stepwave patterns are again visible. z scale in nm.

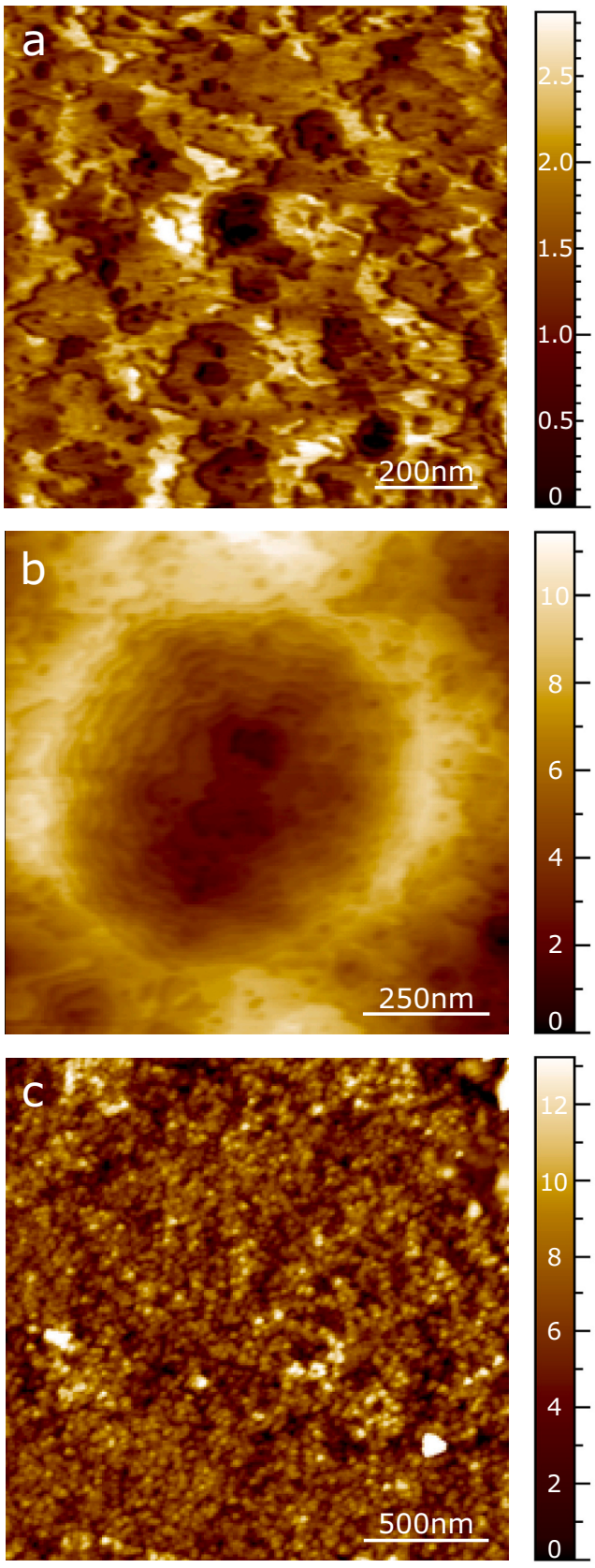

Fig. 8. AFM image of biotite (001) surface after reaction with a-b) 0.1 mol L^{-1} oxalic acid at 40°C for 72 h; c) 0.1 mol L^{-1} oxalic acid at 70°C for 24 h. Dendritic dissolution features (a), pseudo-hexagonal pit displaying a dissolution stepwave configuration (b) and nanoparticle precipitation (c) were observed. z scale in nm.

with organic and inorganic solutions) whereas biotite basal surface was strongly affected by etch pit nucleation, growth, and coalescence when only reacting with oxalic acid. In the nitric acid solution, biotite surface etching was revealed by AFM at 70°C. The size of the etch pits was between 20 and 50 nm with a depth of ~3 nm, i.e., about 3 mica layers (Fig. 4). Hence, the etch pits became undetectable at the meso- and micro-scale (see also Cappelli et al., 2013, 2020).

There were two main differences observed for the tested micas dissolving in oxalic acid solution: (1) a diverse population of rounded and (pseudo)hexagonal etch pits of different sizes were observed on the biotite (001) surface and, dependent upon the experimental conditions, whereas triangular shaped etch pits predominantly developed on the phlogopite surface (sometimes combining into a pseudo hexagonal shaped structure); and (2) the biotite edge surfaces exhibit highly heterogeneous dissolution features whereas the phlogopite generally exhibited step edge surface retreat consistent with morphology observed for dissolution in oxalic-free solutions.

The low Fe amount in the phlogopite chemical composition is likely a factor that determines the differences observed in this study between biotite and phlogopite (biotite Mg-endmember) dissolution patterns. According to previous studies (Hoda and Hood, 1972; Murakami et al., 2003), phlogopite undergoes a vermiculization process in the early stages of the weathering process (loss of K). Preferential leaching of interlayer K and hydration occur without a significant alteration of the chemical and structural composition of the 2:1 layers (Kalinowski and Schweda, 1996). This makes phlogopite more stable compared to biotite due to the lower dissolution rate associated with vermiculite layers (Murakami et al., 2003). The oxidation of the structural Fe(II) in biotite probably takes place concomitantly to the mineral exfoliation. The ejection of octahedral cations (Mg and Fe) and the loss of interlayer K have been identified as the main processes balancing the charge excess (Jeong and Kim, 2003). At the same time, oxidized biotite gains a K-retention capability that prevents significant vermiculization which, to the contrary, is favored by K exchange with hydrated cations during phlogopite alteration (Velde and Meunier, 2008).

In general, phlogopite bulk dissolution rates have been found to be one to two orders of magnitude lower than those of biotite in acidic pH (Clemency and Lin, 1981; Acker and Bricker, 1992; Kalinowski and Schweda, 1996; Malmström and Banwart, 1997; Taylor et al., 2000). In this study, the calculated step-retreat rate of phlogopite was three orders of magnitude lower than the derived value for biotite at pH 1 (HNO_3 and 100°C) (see section 3.1 in Results). Hence, the slower phlogopite dissolution rate and the absence of layer swelling and peeling may be related to the lower Fe content per unit cell of this mica, and thereby resulting in lower reactivity. It should be noted that under this condition the mica vermiculization does not necessarily lead to an overall expansion of the crystal (Velde and Meunier, 2008).

For the set of biotite dissolution tests, it is interesting to note that the high reactivity of the biotite edge surface in the presence of nitric acid may explain the apparent incongruency between the observations at *meso*, micro and nanoscale. The relative rapid dissolution kinetics of the iron-rich mica leads to an enhanced retreat of pre-existing steps, preventing the nucleated etch pits from growing and being detected by interferometry or LCM-DIM. Moreover, layer curling might also be hindering the etch pit development (Turpault and Trotignon, 1994).

Faster retreat of pre-existing steps than etch pit formation (at specific experimental conditions), and the different observation scales used in previous experimental studies may explain why mica basal surface reactivity is reported by a relatively small number of studies (e.g. Adushin et al. (2006), phlogopite dissolution at 125°C and pH 1.5 (HNO_3); Kurganskaya et al. (2012), muscovite dissolution at 155°C and pH 9.4 (NaOH); Pachana et al. (2012), biotite and muscovite dissolution at 200°C and pH 3.3 (HCl); Haward et al. (2011), 10–35°C and pH 1.3–2.1 (oxalic acid); Cappelli et al. (2020) biotite dissolution at 25–70°C and pH 1.3–2.1 (oxalic acid)).

4.2. Dissolution features

During mica dissolution under acidic pH conditions, three main morphological changes were identified: 1) the swelling, peeling, and/or creasing of layers – only for biotite; 2) the increase of the (001) surface roughness due to: a) the nucleation and growth of etch pits – for biotite in oxalic acid solution and phlogopite – and b) the formation of dissolution channels – for both micas; and 3) the retreat of pre-existing steps – for both micas.

The primary results for each point are discussed as follows:

1) As described above and in previous works (Turpault and Trotignon, 1994; Cappelli et al., 2013; Cappelli et al., 2020), biotite layers may experience a swelling process from the step edge leading to a subsequent layer peel-off when dissolving in acidic solution. The processes that likely induce the observed swelling and peeling-off of altered biotite layers are: the hydration of the layer, the preferential leaching of K, Mg, Fe, and Al, and the formation of a condensed Si-rich (possibly amorphous) phase smaller in volume with respect to the unreacted material (Turpault and Trotignon, 1994). In contrast, the LCM-DIM observations of biotite alteration in oxalic acid solutions reveal that layer peeling-off does not tend to take place along the dendritic features emanating from the step edges. Interestingly, however, when relatively large hexagonal etch pits formed, a general creasing of the biotite surface delimited by the etch pit edges was visible (Fig. 5). The altered layer dissolves leaving a pristine surface and a well-defined hexagonal-shaped structure (see Supplementary material, LCM-DIM-Movie1, and LCM-DIM-Movie2).

2) Etch pit populations with different sizes formed on the (001) surface of phlogopite and biotite during dissolution with both (organic and inorganic) acids. In this regard, the formation of ligand-surface complexes (Welch and Ullman, 1993; Pokrovsky et al., 2005; Cama and Ganor, 2006; Olsen and Rimstidt, 2008; Haward et al., 2011; Shao et al., 2011a) and ligand-cation complexes in solution (Barman et al., 1992; Oelkers and Schott, 1998; Oelkers and Gislason, 2001; Wang et al., 2005; Golubev et al., 2006; Tu et al., 2007; Ramos et al., 2014) may be affecting the kinetics of the etch pits formation and growth. Atomistic and molecular modelling is needed to describe the possible elementary reactions taking place on the mica interface and to better understand the role that ligand-cation complexion has on the etch pit formation processes.

Triangular-shaped etch pits on the phlogopite basal surfaces sometimes followed trench patterns (Fig. 3c,d). An arrangement of etch pits was observed on the (001) surface of muscovite under different experimental conditions (i.e., pH 9.4 and T 155°C) (Shao et al., 2010; Kurganskaya et al., 2012). Channel-like features were also observed on biotite surfaces during dissolution in nitric acidic conditions (see Fig. SI8b,c). Brandt et al. (2003) observed comparable dissolution structures during chlorite dissolution at 25°C in acidic pH (HCl) and ascribed its formation to the initial existence of cracks in the sample top layers. Moreover, defects and zones of prevalent isomorphic substitution could generate areas with a higher reactivity promoting the etching of the surface. However, a crystallographic control over the development of channels (and etch pit trenches) cannot be excluded (see for example Fig. 2d). In addition, in some areas, dissolution took place underneath the upper layers (darker regions in Fig. 2b) pointing to the existence of localized and particularly reactive fronts, from which dissolution channels opened and spread under less reactive layers.

Crystal lattice distortion and dislocation stress energy can cause mineral surface defects from which etch pits can easily develop (Blum et al., 1990). The different-sized etch pits that formed on the (001) surface of biotite in response to reactions in the presence of oxalic acid solution (Fig. 6-8) may be attributed to different defects and to direction and velocity of the steps generated from these features (Kurganskaya and Rohlfs, 2020). For example, point defects and screw dislocations are sources of monolayer and deep waves of steps, respectively (Kurganskaya et al., 2012; Kurganskaya and Luttge, 2021). Likewise, the overall configuration of the biotite surface depicted at a certain point of the dissolution reaction is the combination of the pre-existing step retreat, etch pit nucleation, and stepwaves spreading and coalescence, which shape the surface at any given moment.

3) The layer edge reactivity of biotite in nitric acid solution is site-specific at the beginning of dissolution, but as the reaction progresses steps start to retreat almost uniformly (Cappelli et al., 2013). Similar behavior was observed for phlogopite in both organic and inorganic solutions. This observed dissolution behavior and resulting characteristics agree well with the general kinetic theoretical model proposed by Lasaga and Lüttge (2004a, 2004b). However, when biotite reacts with oxalic acid, edge dissolution showed more complex branching and dendritic features.

One possible explanation that could account for the biotite edge surface branching dissolution is based on the interaction between mineral surface and solution ligands (Axe and Persson, 2001; Johnson et al., 2004; Kang and Xing, 2007; Ramos et al., 2014; Ward and Brady, 1998). At pH $\leq$ 3, ionic species of the organic ligand (single protonated (HOx^-) and fully deprotonated (Ox^{2-})) can form inner-sphere surface complexes with tetrahedral (>AlOH and > $AlOH_2^+$) and octahedral (>Mg-FeOH and > Mg-$FeOH_2^+$) edge surface groups (Ganor et al., 2009). The possible different kinetics associated with proton (H^+ adsorption)-induced or ligand (oxalic adsorption)-induced dissolution could lead to irregular step edge features.

Importantly, the ligand-cation complexation is site-specific (organic ligands preferentially adsorb on specific reactive sites) and, for aluminosilicate, Al surface sites are probably more prone to form complexes with the oxalate (Ganor et al., 2009). In addition, in iron-rich minerals, such as biotite, the Fe-ligand complexes may play an important role in the dissolution process. The oxidized structural iron of biotite forms stable Fe(III)-ligand surface complexes with a high desorption activation energy (low dissolution rate) (Panias et al., 1996). This could lead to a temporal reactive surface site blocking (from an H^+ attack) that prevents further mineral dissolution. The difference in the complex kinetics release becomes less pronounced at higher temperatures (Panias et al., 1996), and could explain why the branching edge feature (dendritic shape) at low temperature (25°C) turned to jugged shape (shorter branches) at higher temperature (>40°C) (data not shown) (i.e., higher temperatures promote cation-oxalate complex desorption and thus more homogeneous edge face dissolution). A similar effect was observed with the variation of oxalic acid whereby higher concentration induces a jugged-shaped edge dissolution pattern (Fig. 7f). However, this behavior is attributed to the higher contribution of the ligand-promoted dissolution given the increase of the surface complexes per reactive sites (Ganor et al., 2009).

A second phenomenon that may lead to the heterogeneous biotite edge surface dissolution, in the presence of oxalic acid, is related to the local saturation state, especially near the layer edges (Murakami et al., 2003; Shao et al., 2010; Hu et al., 2011). In agreement with Murakami et al. (2003), when supersaturation is achieved, released cations will precipitate before diffusing into the bulk solution. In the case of biotite alteration, the initial K^+-H^+ exchange, the edge and interlayer surface protonation, and the resulting structure hydrolysis could lead to a high solution concentration of ligand-cation complexes (Al, Mg, Fe-Ox) thereby promoting local supersaturation in spite of bulk solution undersaturation. In saturated micro-environments, oxalate salts could form under acidic conditions (Pérez et al., 2009; Rozalen and Huertas, 2013). Mg-oxalate and Fe-oxalate could precipitate on step edges and the basal surface thereby blocking surface reaction sites. Hence, dissolution can only take place at unblocked reaction site regions, leading to step retreat around the coated areas and the formation of branching features. In some instances, AFM and VSI images show secondary phase precipitates on the (001) surface or along layer edges (Fig. 8c and Fig. SI11), supporting this model for heterogeneous dissolution.

The fact that phlogopite dissolution does not show branched-type features may be ascribed to its more stable structure and the kinetics

mostly associated with the prevalent Mg-ligand surface complex. Moreover, local supersaturation is not expected to result from the slower dissolution rates associated with the biotite Mg-endmember. Consistent with reasoning, precipitates were only observed sporadically on the phlogopite (001) surface during the reaction with nitric acid (pH 2) at 100°C (Fig. SI5), whereas secondary phases were never observed on the edge surfaces, always dissolving parallel to the step line.

5. Conclusions

The changes in the morphological and topographical features of biotite and phlogopite basal surfaces reacting with nitric and oxalic acid solutions (pH ~ 1–2) were monitored using three complementary microscopy techniques. Mesoscale in situ observations of mica basal surfaces using LCM-DIM provided topographic data to elucidate the overall dissolution process. Interferometry and AFM were used to study and characterize the dissolution features in detail, at both the micro and nano-scales. A combination of data obtained from these techniques provides an integrated and comprehensive description of the dissolution dynamics of mica surfaces, as well as allows for a more robust differentiation of the effects of (in)organic acids on mica reactivity. The main findings of this study are summarized as follows:

- Mica dissolution is driven by the alteration of preexisting steps and the nucleation of etch pits. Within the acidic range tested, oxalic acid induces etch pit development and nitric acid contributes to edge face dissolution and the formation of altered layer rims. The evolution of these processes likely depends upon the Fe/Mg ratio, which may be responsible for the different mica reactivities.
- In general, the lower the pH and higher the temperature, the faster the mica dissolution. In oxalic acid solutions, an increase in the concentration of the acid in the solution and in the temperature leads to an increase in etch pit density on both mica surfaces, but more drastically affects the surface morphology of biotite.
- Dissolution features observed during mica dissolution (e.g., hexagonal etch pits, dendritic structures) depend on the kinetics and thermodynamics of the overall reactions and on the local chemistry and structure of the mineral-solution interface. Molecular modelling of the mineral-interface dynamics observed in this study will help deduce the mechanisms and kinetic parameters that control mica reactivity.

Supplementary data to this article can be found online at https://doi.org/10.1016/j.clay.2023.106923.

CRediT authorship contribution statement

Chiara Cappelli: Conceptualization, Methodology, Investigation, Writing – original draft. **Alexander E.S. Van Driessche:** Conceptualization, Validation, Writing – review & editing. **Jordi Cama:** Conceptualization, Validation, Writing – review & editing. **F. Javier Huertas:** Conceptualization, Writing – review & editing, Funding acquisition.

Declaration of Competing Interest

The authors declare that they have no known competing financial interests or personal relationships that could have appeared to influence the work reported in this paper.

Data availability

The data have been included either in the main text or in the supplementary material. Further specifications on the methodology and/or results will be provided upon request.

Acknowledgements

This research was financially supported by the CGL2011–22567, CGL2014–55108-P, CGL2016–78783–C2-R, CGL2017–82331-R and CEX2018–000794-S projects (Spanish Ministry of Science and Innovation) and the Catalan project 2021 SGR 00308. IDAEA-CSIC is a Severo Ochoa Centre of Excellence (Spanish Ministry of Science and Innovation, Project CEX2018-000794-S). The authors thank Dr. Geoffrey Tick for assistance in the English editing of the text and the reviewers for the useful comments and suggestions. FJH, amdg.

References

Acker, J.G., Bricker, O.P., 1992. The influence of pH on biotite dissolution and alteration kinetics at low temperature. Geochim. Cosmochim. Acta 56, 3073–3092.
Aoudjit, H., Elsass, F., Robert, M., Righi, D., 1996. Mica weathering in acidic soils by analytical electron microscopy. Clay Miner. 31, 319–332.
Arocena, J.M., Velde, B., Robertson, S.J., 2012. Weathering of biotite in the presence of arbuscular mycorrhizae in selected agricultural crops. Appl. Clay Sci. 64, 12–17.
Axe, K., Persson, P., 2001. Time-dependent surface speciation of oxalate at the water-boehmite (γ-AlOOH) interface: implications for dissolution. Geochim. Cosmochim. Acta 65, 4481–4492.
Balland-Bolou-Bi, C., Bolou-Bi, E.B., Vigier, N., Mustin, C., Poszwa, A., 2019. Increased Mg release rates and related Mg isotopic signatures during bacteria-phlogopite interactions. Chem. Geol. 506, 17–28.
Barman, A.K., Varadachari, C., Ghosh, K., 1992. Weathering of silicate minerals by organic acids. I. Nature of cation solubilisation. Geoderma 53, 45–63.
Blum, A.E., Yund, R.A., Lasaga, A.C., 1990. The effect of dislocation density on the dissolution rate of quartz. Geochim. Cosmochim. Acta 54, 283–297.
Bonneville, S., Morgan, D.J., Schmalenberger, A., Bray, A., Brown, A., Banwart, S.A., Benning, L.G., 2011. Tree-mycorrhiza symbiosis accelerate mineral weathering: Evidences from nanometer-scale elemental fluxes at the hypha–mineral interface. Geochim. Cosmochim. Acta 75, 6988–7005.
Brandt, F., Bosbach, D., Krawczyk-Bärsch, E., Arnold, T., Bernhard, G., 2003. Chlorite dissolution in the acid ph-range: a combined microscopic and macroscopic approach. Geochim. Cosmochim. Acta 67, 1451–1461.
Cama, J., Ganor, J., 2006. The effects of organic acids on the dissolution of silicate minerals: a case study of oxalate catalysis of kaolinite dissolution. Geochim. Cosmochim. Acta 70, 2191–2209.
Cappelli, C., Van Driessche, A.E.S., Cama, J., Huertas, F.J., 2013. In situ observation of biotite dissolution at pH 1 using advanced optical microscopy. Cryst. Growth Des. 13, 2880–2886.
Cappelli, C., Lamarca-Irisarri, D., Camas, J., Huertas, F.J., Van Driessche, A.E., 2015. In situ observation of biotite (001) surface dissolution at pH 1 and 9.5 by advanced optical microscopy. Beilstein J. Nanotechnol. 6, 665–673.
Cappelli, C., Cama, J., Van Driessche, A.E.S., Huertas, F.J., 2020. Biotite reactivity in nitric and oxalic acid at low temperature and acid pH from surface and bulk dissolution measurements. Chem. Geol. 554, 119806.
Clemency, C.V., Lin, F.-C., 1981. Dissolution kinetics of phlogopite; II, Open system using an ion-exchange resin. Clay Clay Miner. 29, 107–112.
Ganor, J., Reznik, I.J., Rosenberg, Y.O., 2009. Organics in Water-Rock Interactions. Rev. Mineral. Geochem. 70 (1), 259–369.
Garcia, D.J., Shao, H., Hu, Y., Ray, J.R., Jun, Y.-S., 2012. Supercritical CO2-brine induced dissolution, swelling, and secondary mineral formation on phlogopite surfaces at 75-95 [degree]C and 75 atm. Energy Environ. Sci. 5, 5758–5767.
Golubev, S.V., Bauer, A., Pokrovsky, O.S., 2006. Effect of pH and organic ligands on the kinetics of smectite dissolution at 25° C. Geochim. Cosmochim. Acta 70, 4436–4451.
Haward, S.J., Smits, M.M., Ragnarsdóttir, K.V., Leake, J.R., Banwart, S.A., McMaster, T. J., 2011. In situ atomic force microscopy measurements of biotite basal plane reactivity in the presence of oxalic acid. Geochim. Cosmochim. Acta 75, 6870–6881.
Hoda, S.N., Hood, W.C., 1972. Laboratory alteration of trioctahedral micas. Clay Clay Miner. 20, 343–358.
Hodson, M.E., 2006. Does reactive surface area depend on grain size? Results from pH 3, 25°C far-from-equilibrium flow-through dissolution experiments on anorthite and biotite. Geochim. Cosmochim. Acta 70, 1655–1667.
Hu, Y., Ray, J.R., Jun, Y.-S., 2011. Biotite–brine interactions under acidic hydrothermal conditions: fibrous Illite, goethite, and kaolinite formation and biotite surface cracking. Environ. Sci. Technol. 45, 6175–6180.
Jeong, G.Y., Kim, H.B., 2003. Mineralogy, chemistry, and formation of oxidized biotite in the weathering profile of granitic rocks. Am. Mineral. 88, 352–364.
Johnson, S.B., Yoon, T.H., Slowey, A.J., Brown, G.E., 2004. Adsorption of organic matter at mineral/water interfaces: 3. Implications of surface dissolution for adsorption of oxalate. Langmuir 20, 11480–11492.
Kalinowski, B.E., Schweda, P., 1996. Kinetics of muscovite, phlogopite, and biotite dissolution and alteration at pH 1-4, room temperature. Geochim. Cosmochim. Acta 60, 367–385.
Kang, S., Xing, B., 2007. Adsorption of Dicarboxylic Acids by Clay Minerals as Examined by in Situ ATR-FTIR and ex Situ DRIFT. Langmuir 23, 7024–7031.
Kaviratna, H., Pinnavaia, T.J., 1994. Acid hydrolysis of octahedral Mg^{2+} sites in 2:1 layered silicates; an assessment of edge attack and gallery access mechanisms. Clay Clay Miner. 42, 717–723.

Kurganskaya, I., Luttge, A., 2013. A comprehensive stochastic model of phyllosilicate dissolution: Structure and kinematics of etch pits formed on muscovite basal face. Geochim. Cosmochim. Acta 120, 545–560.
Kurganskaya, I., Luttge, A., 2021. Mineral Dissolution Kinetics: Pathways to Equilibrium. ACS Earth Space Chem. 5 (7), 1657–1673.
Kurganskaya, I., Rohlfs, R.D., 2020. Atomistic to meso-scale modeling of mineral dissolution: Methods, challenges and prospects. Am. J. Sci. 320, 1–26.
Kurganskaya, I., Arvidson, R.S., Fischer, C., Luttge, A., 2012. Does the stepwave model predict mica dissolution kinetics? Geochim. Cosmochim. Acta 97, 120–130.
Lasaga, A.C., Luttge, A., 2001. Variation of crystal dissolution rate based on a dissolution stepwave model. Science 291, 2400–2404.
Lasaga, A.C., Lüttge, A., 2004a. Mineralogical approaches to fundamental crystal dissolution kinetics. Am. Mineral. 89, 527–540.
Lasaga, A.C., Lüttge, A., 2004b. Mineralogical approaches to fundamental crystal dissolution kinetics - dissolution of an A3B structure. Eur. J. Mineral. 16, 713–729.
Li, T., Wang, H., Zhou, Z., Chen, X., Zhou, J., 2015. A nano-scale study of the mechanisms of non-exchangeable potassium release from micas. Appl. Clay Sci. 118, 131–137.
Luttge, A., Arvidson, R.S., Fischer, C., Kurganskaya, I., 2019. Kinetic concepts for quantitative prediction of fluid-solid interactions. Chem. Geol. 504, 216–235.
Malmström, M., Banwart, S., 1997. Biotite dissolution at 25°C: the pH dependence of dissolution rate and stoichiometry. Geochim. Cosmochim. Acta 61, 2779–2799.
McMaster, T.J., Smits, M.M., Haward, S.J., Leake, J.R., Banwart, S., Ragnarsdottir, K.V., 2008. High-resolution imaging of biotite dissolution and measurement of activation energy. Mineral. Mag. 72, 115–120.
Min, Y., Kim, D., Jun, Y.-S., 2018. Effects of Na+ and K+ exchange in interlayers on biotite dissolution under high-temperature and high-CO2-pressure conditions. Environ. Sci. Technol. 52, 13638–13646.
Murakami, T., Utsunomiya, S., Yokoyama, T., Kasama, T., 2003. Biotite dissolution processes and mechanisms in the laboratory and in nature: early stage weathering environment and vermiculitization. Am. Mineral. 88, 377–386.
Niu, H., Kinnunen, P., Sreenivasan, H., Adesanya, E., Illikainen, M., 2020. Structural collapse in phlogopite mica-rich mine tailings induced by mechanochemical treatment and implications to alkali activation potential. Miner. Eng. 151, 106331.
Oelkers, E.H., Gislason, S.R., 2001. The mechanism, rates and consequences of basaltic glass dissolution: I. An experimental study of the dissolution rates of basaltic glass as a function of aqueous Al, Si and oxalic acid concentration at 25°C and pH = 3 and 11. Geochim. Cosmochim. Acta 65, 3671–3681.
Oelkers, E.H., Schott, J., 1998. Does organic acid adsorption affect alkali-feldspar dissolution rates? Chem. Geol. 151, 235–245.
Olsen, A.A., Rimstidt, J.D., 2008. Oxalate-promoted forsterite dissolution at low pH. Geochim. Cosmochim. Acta 72, 1758–1766.
Ottolini, L.P., Schingaro, E., Scordari, F., Mesto, E., Lacalamita, M., 2010. The role of SIMS in the investigation of the complex crystal chemistry of mica minerals. IOP Conf. Ser. 7, 012023.
Panias, D., Taxiarchou, M., Paspaliaris, I., Kontopoulos, A., 1996. Mechanisms of dissolution of iron oxides in aqueous oxalic acid solutions. Hydrometallurgy 42, 257–265.
Pérez, M.A., Cabrera, A.B., Silva, R., Mendoza, M.E., Carrillo, J.L., 2009. Patterns of aggregation in coprecipitation reactions. Rev. Mexicana Física 55, 90–96.
Pinzari, F., Cuadros, J., Napoli, R., Canfora, L., Baussà Bardají, D., 2016. Routes of phlogopite weathering by three fungal strains. Fungal Biol. 120, 1582–1599.
Pokrovsky, O.S., Schott, J., Castillo, A., 2005. Kinetics of brucite dissolution at 25°C in the presence of organic and inorganic ligands and divalent metals. Geochim. Cosmochim. Acta 69, 905–918.
Ramos, M.E., Garcia-Palma, S., Rozalen, M., Johnston, C.T., Huertas, F.J., 2014. Kinetics of montmorillonite dissolution: an experimental study of the effect of oxalate. Chem. Geol. 363, 283–292.
Rozalen, M., Huertas, F.J., 2013. Comparative effect of chrysotile leaching in nitric, sulfuric and oxalic acids at room temperature. Chem. Geol. 352, 134–142.
Rufe, E., Hochella, M.F., 1999. Quantitative assessment of reactive surface area of phlogopite during acid dissolution. Science 285, 874–876.
Said, A., Zhang, Q., Qu, J., Liu, Y., Lei, Z., Hu, H., Xu, Z., 2018. Mechanochemical activation of phlogopite to directly produce slow-release potassium fertilizer. Appl. Clay Sci. 165, 77–81.
Schabernack, J., Kurganskaya, I., Fischer, C., Luttge, A., 2021. Influence of muscovite (001) surface nanotopography on radionuclide adsorption studied by Kinetic Monte Carlo simulations. Minerals 11, 468.
Schliemann, R., Churakov, S.V., 2021. Atomic scale mechanism of clay minerals dissolution revealed by ab initio simulations. Geochim. Cosmochim. Acta 293, 438–460.
Shao, H., Ray, J.R., Jun, Y.-S., 2010. Dissolution and precipitation of clay minerals under geologic CO2 sequestration conditions: CO2−brine−phlogopite interactions. Environ. Sci. Technol. 44, 5999–6005.
Shao, H., Ray, J.R., Jun, Y.-S., 2011a. Effects of organic ligands on supercritical CO2-induced phlogopite dissolution and secondary mineral formation. Chem. Geol. 290, 121–132.
Shao, H., Ray, J.R., Jun, Y.-S., 2011b. Effects of salinity and the extent of water on supercritical CO2-induced phlogopite dissolution and secondary mineral formation. Environ. Sci. Technol. 45, 1737–1743.
Studenroth, S., Huber, S.G., Kotte, K., Schöler, H.F., 2013. Natural abiotic formation of oxalic acid in soils: results from aromatic model compounds and soil samples. Environ. Sci. Technol. 47, 1323–1329.
Taylor, A.S., Blum, J.D., Lasaga, A.C., MacInnis, I.N., 2000. Kinetics of dissolution and Sr release during biotite and phlogopite weathering. Geochim. Cosmochim. Acta 64, 1191–1208.
Tu, S.-X., Guo, Z.-F., Sun, J.-H., 2007. Effect of oxalic acid on potassium release from typical chinese soils and minerals. Pedosphere 17, 457–466.
Turpault, M.P., Trotignon, L., 1994. The dissolution of biotite single crystals in dilute HNO3 at 24°C: evidence of an anisotropic corrosion process of micas in acidic solutions. Geochim. Cosmochim. Acta 58, 2761–2775.
Van Driessche, A.E.S., Sleutel, M., 2013. In situ measurement of crystal surface dynamics in pure and contaminated solutions by Confocal Microscopy and Atomic Force Microscopy. Cryst. Res. Technol. 48, 919–941.
Velde, B., Meunier, A., 2008. Clay mineral formation in weathered rocks: water/rock interaction. In: Velde, B., Meunier, A. (Eds.), The Origin of Clay Minerals in Soils and Weathered Rocks. Springer, Berlin Heidelberg, Berlin, Heidelberg, pp. 143–239.
Voinot, A., Lemarchand, D., Collignon, C., Granet, M., Chabaux, F., Turpault, M.P., 2013. Experimental dissolution vs. transformation of micas under acidic soil conditions: Clues from boron isotopes. Geochim. Cosmochim. Acta 117, 144–160.
Wang, X., Li, Q., Hu, H., Zhang, T., Zhou, Y., 2005. Dissolution of kaolinite induced by citric, oxalic, and malic acids. J. Colloid Interface Sci. 290, 481–488.
Ward, D.B., Brady, P.V., 1998. Effect of Al and organic acids on the surface chemistry of kaolinite. Clay Clay Miner. 46, 453–465.
Welch, S.A., Ullman, W.J., 1993. The effect of organic acids on plagioclase dissolution rates and stoichiometry. Geochim. Cosmochim. Acta 57, 2725–2736.
Wu, H., Qiang, S., Fan, Q., Zhao, X., Liu, P., Li, P., Liang, J., Wu, W., 2018. Exploring the relationship between Th(IV) adsorption and the structure alteration of phlogopite. Appl. Clay Sci. 152, 295–302.
Zhang, L., Kim, D., Kim, Y., Wan, J., Jun, Y.-S., 2017. Effects of phosphate on biotite dissolution and secondary precipitation under conditions relevant to engineered subsurface processes. Phys. Chem. Chem. Phys. 19, 29895–29904.